

Manipulating anthracyclines for deeper tissue penetration and implications for glycolytic tissues

Abels, E.R.; Linden, E. ter; Rohling, J.H.T.; Voortman, L.M.; Janssen, L.; Hornsveld, M.; ...; Neefjes, J.J.C.

Citation

Abels, E. R., Linden, E. ter, Rohling, J. H. T., Voortman, L. M., Janssen, L., Hornsveld, M., ... Neefjes, J. J. C. (2025). Manipulating anthracyclines for deeper tissue penetration and implications for glycolytic tissues. *Proceedings Of The National Academy Of Sciences*, 122(36). doi:10.1073/pnas.2510263122

Version: Publisher's Version

License: Creative Commons CC BY-NC-ND 4.0 license

Downloaded from: https://hdl.handle.net/1887/4281094

Note: To cite this publication please use the final published version (if applicable).



Manipulating anthracyclines for deeper tissue penetration and implications for glycolytic tissues

Erik R. Abels^{a,1}, Esther ter Linden^{a,1}, Jos H. T. Rohling^a D, Lennard M. Voortman^a, Lennert Janssen^a, Marten Hornsveld^a, Herman S. Overkleeft^b, Sabina Y. van der Zanden^a, Marike L. D. Broekman^{a,c,d}, and Jacques Neefjes^{a,2}

Affiliations are included on p. 11.

Edited by Hidde Ploegh, Boston Children's Hospital, Boston, MA; received April 25, 2025; accepted July 31, 2025

How drugs penetrate tissues is poorly understood yet important, since drugs that fail to reach their target will be ineffective. We followed the fate of anthracycline cancer drugs at high resolution by exploiting their intrinsic fluorescence. In a cell-based spheroid model, the soluble compound fluorescein penetrates the entire spheroid, unlike hydrophobic fluorescent lipids, which only enter the outermost cell layer. Anthracyclines have intermediate hydrophobicity. They enter the nucleus of a few outer cell layers at neutral pH, but penetrate the spheroids more deeply under acidic conditions, with a reduction in cell entry and cytotoxicity. The glycolytic conditions that prevail in the tumor microenvironment may thus limit cell entry and contribute to anthracycline drug resistance. We evaluated a library of anthracycline variants to determine the physicochemical properties related to tissue penetration depth. We find that this is determined by only three chemical properties: molar refractivity, topological polar surface area, and water solubility. Our findings suggest that modifications of anthracyclines may improve access and activity to deeply tissue-embedded targets such as pancreatic cancer.

anthracyclines | doxorubicin | tissue penetration | glycolysis | drug resistance

Most anticancer drugs are given intravenously and are distributed across the body via the circulation. To be clinically effective, these drugs must then leave the circulation and enter tissues to access their intended targets. Drugs can be distributed by diffusion and/or convection (1, 2). Extracellular structural features may influence drug transport across tissues. The tissue microenvironment is best studied for tumors and can affect the diffusion of drugs, for example, by their binding to extracellular matrix components. The structure and density of tissues can likewise impact free diffusion of drugs between cells (3). Lymphatic draining of target tissues and the presence or absence of drug importers and exporters further contribute to drug distribution. Because most drugs are not fluorescent and therefore difficult to detect noninvasively, understanding drug penetration in tissues at high spatial resolution remains a challenge.

We focus on anthracyclines, drugs that are intrinsically red fluorescent. The different anthracycline cancer drugs in clinical use all have a similar architecture: a hydrophobic tetracycline conjugated ring system connected to a weakly basic amino sugar. Doxorubicin is their best-known member and for the treatment of many blood and solid tumors (4–6). Most anthracyclines rely on at least two cytotoxic mechanisms: They poison the enzyme topoisomerase II to generate DNA double-strand breaks, and they evict nucleosomes from chromatin by intercalation into DNA at particular regions in the genome (5, 7, 8). Of these two mechanisms, nucleosome eviction is the most cytotoxic (7). We identified and generated anthracycline variants only inducing nucleosome eviction, drugs such as dimethyldoxorubicin and aclarubicin (6, 7, 9, 10). Dimethyldoxorubicin has the same tissue distribution as doxorubicin while aclarubicin prefers location in blood organs such as spleen, lymph nodes, and bone marrow (7). These drugs control tumor growth in vitro and in vivo but lack two of the treatment-limiting side effects; accumulated dose-dependent cardiotoxicity and therapy-induced second tumors (7). This implies that these drugs can be used more chronically at lower toxicity, resulting in a higher Quality of Life to cancer

Tissue penetration of doxorubicin in vivo is limited (11–13). The permeable nature of the tumor neovasculature may promote more efficient access of anthracyclines to tumor tissues (14). Various technologies have been tested to improve doxorubicin tissue penetration. These include focused ultrasound to open tight junctions between endothelial cells (15). Also, ionization radiation and pressurization of intraperitoneal aerosols can increase tissue penetration of doxorubicin (16). Tissues are not homogeneous. The behavior and distribution of anthracyclines are affected by areas that contain many stromal cells

Significance

Anthracyclines including doxorubicin are used by over 1 million cancer patients annually. Various tumors respond to these drugs, while others, such as pancreatic cancer, do not. We used the intrinsic fluorescence properties of these drugs to follow their tissue penetration over time and space. Doxorubicin and the other clinically used anthracyclines show limited tissue penetration at physiological pH. Under acidic glycolytic conditions, the single amine in these drugs is protonated and prevents efficient uptake, causing drug resistance. We used a library of anthracycline variants to identify chemical features that improve tissue penetration. We define modifications in anthracyclines allowing cell entry under glycolytic conditions. The concepts defined here support the design of anthracycline drugs that act at tumors currently inaccessible.

Competing interest statement: J.N. is a shareholder in NIHM that aims to produce aclarubicin for clinical use.

This article is a PNAS Direct Submission.

Copyright © 2025 the Author(s). Published by PNAS. This article is distributed under Creative Commons Attribution-NonCommercial-NoDerivatives License 4.0 (CC BY-NC-ND).

¹E.R.A. and E.t.L. contributed equally to this work.

²To whom correspondence may be addressed. Email: j.j.c.neefjes@lumc.nl.

This article contains supporting information online at https://www.pnas.org/lookup/suppl/doi:10.1073/pnas. 2510263122/-/DCSupplemental.

Published September 3, 2025.

and that are rich in extracellular matrix, high in expression of drug transporters, acidified (glycolytic) areas, necrotic areas, and different blood vessel densities (17). The intrinsic fluorescent properties of anthracyclines allowed a visualization of their tissue penetration at high temporal and spatial resolution without the need of further modifications (18, 19). In tumor sections, doxorubicin penetrated only a few perivascular cell layers in human breast cancer tissue (12). Pancreatic cancer is a tumor that poorly responds to doxorubicin-based treatments, even though pancreatic cancer organoids are highly sensitive to these drugs (20, 21). This may be caused by the insulating fibroblast layer separating the tumor from blood vessels that provide the drugs. These fibroblasts are also known to modulate tumor immune responses. The oxygen poor regions induce a shift to glycolytic conditions. As a result, the cells secrete acetate and acidify the tissue microenvironment including that of pancreatic tumors (22, 23). Understanding drug distribution is therefore essential to arrive at effective drugs.

Here, we studied tissue distribution of a series of anthracyclines in clinical use and new anthracycline variants. We applied high-resolution confocal fluorescence microscopy on spheroids to examine penetration of anthracyclines. We establish rules for tissue penetration and identify a more strongly glycolytic environment as an effective drug resistance mechanism. Drug penetration is determined by surprisingly few chemical features. These provide the basis for modification of anthracycline drugs for better tissue penetration, important for tumors such as pancreatic cancer. Many other (nonfluorescent) drugs contain primary amines and possibly obey the same rules for tissue penetration, cell entry, and drug resistance, as defined here for anthracyclines.

Results

The Hydrophobic Nature of a Compound Determines Its Penetration Into Spheroids. To follow tissue penetration of fluorescent compounds, we used spheroid cultures that form a dense cellular assembly for imaging by time-lapse spinning disk microscopy. The spheroids consist of pancreatic stellate cells (RLT-PSC) that constitutively express NLS-iRFP to mark their nucleus(24). Drug penetration was visualized using line scan analysis and by dividing the cross-section of spheroids into different compartments (bins). This allows quantification of fluorescent molecules in real time in viable tissue. We quantified drug fluorescence (normalized to compound concentration) within the different spheroid layers (Fig. 1A). First, we selected three different fluorescent molecules: water-soluble fluorescein, the hydrophobic lipid DiOC₁₈, and doxorubicin, which contains a hydrophobic tetracycline and a hydrophilic amino sugar (Fig. 1 A-G). The spheroids were exposed to 2 μ M DiOC₁₈, 2 μ M doxorubicin, or 25.6 μ M fluorescein for 2 h and imaged equatorially (Fig. 1 B–G). The concentration of doxorubicin used in our experiments reflected the serum Cmax of doxorubicin in human patients (25). The distribution of these molecules is markedly different. Fluorescein shows an even distribution across all cell layers (Fig. 1B). DiOC₁₈ only entered the single outer cell layer, ultimately localizing to vesicular structures (Fig. 1C). Doxorubicin entered the nucleus of a few of the outer cell layers while concentrations detected in the spheroid interior were considerably lower (Fig. 1D). A line scan of the spheroids illustrates the distribution of the different compounds (Fig. 1 *E*–*G*).

Modification of Doxorubicin for Better Penetration in Spheroid-**Pancreatic Organoids.** The problem with drugs distributed across the body via the circulation is illustrated by pancreatic cancer, which responds poorly to chemotherapy, including anthracyclines.

These tumors are encapsulated by stromal cells, mostly fibroblasts, and are located at some distance from blood vessels (Fig. 2A). Consequently, anthracyclines must penetrate tissue to access the pancreatic tumor.

To mimic human pancreatic cancer, we examined entry into a pancreatic cancer 3D organoid model of doxorubicin variants, where the amino sugar was modified or absent (Fig. 2B) (7, 9). The model consisted of pancreatic tumor cells [PDX; expressing nuclear H2B-Cerulean (in yellow)] surrounded by fibroblasts [expressing NLS-iRFP720 in the nucleus (in red)] (26) (Fig. 2C). The organoid was exposed to 10 µM of the different doxorubicin variants and then imaged by spinning disk microscopy at an equatorial plane. We scaled the penetration depth of the different drugs and determined their fluorescence/µm²(Fl/µm²) in the different bins, normalized to total drug fluorescence observed as a measure of fluorescence intensity as a proxy for drug concentration (Fig. 2 C-F). The different anthracyclines penetrated the organoid differently. Unlike doxorubicin or the other anthracyclines, azidodoxorubicin and doxorubicinone penetrated deeply into the fibroblast-pancreatic tumor organoids (Fig. 2 D-F). A line plot across the pancreatic tumor organoid coculture (shown in yellow) confirmed that anthracycline structure significantly impacts access to the fibroblast-embedded pancreatic cancer organoids (Fig. 2F). We repeated the anthracycline penetration experiments with spheroids composed of PDX or RLT-PSC cells only (SI Appendix, Figs. S1A and S2A). Again, live cell imaging at an equatorial plane composed of only RLT-PSC cells showed that doxorubicin is acquired predominantly by the outer cell layers without deeper penetration. Fluorescence quantification showed 60 to 80% of doxorubicin fluorescence present in the outer two bins (SI Appendix, Figs. S1 A and B and S2 A and B). Dimethyldoxorubicin fluorescence was higher in the spheroid interior when compared to doxorubicin (Fig. 3 D-I and SI Appendix, Fig. S1 A and B). Images at higher magnification showed the difference in cellular localization of the anthracyclines in the spheroid interior. Azidodoxorubicin and doxorubicinone were distributed across the spheroid, while dimethyldoxorubicin was found in the NLS-iRFP-marked nucleus of cells in the periphery of the spheroid. These drugs failed to enter the nucleus of cells in the spheroid interior (SI Appendix, Fig. S1 A, Insets). Line plot analyses showed colocalization of doxorubicin with the marker NLS-iRFP in the nucleus of the outer cell layer only. Dimethyldoxorubicin also entered the NLS-iRFP-marked nucleus in the spheroid outer cell layers. The fraction of drug that was localized more to the internal regions of the spheroid failed to enter the NLS-iRFP-marked nucleus. Azidodoxorubicin and doxorubicinone penetrated deeply into spheroids while failing to enter NLS-iRFP-marked nuclei (SI Appendix, Fig. S1 C). To determine the impact of spheroid penetration on overall toxicity in a 3D setting, RLT-PSCs grown as spheroids were treated with 10 µM of the different anthracyclines for 2 h. Cell survival was measured 72 h posttreatment using a CellTiter-Glo assay (SI Appendix, Fig. S1D). Toxicity observed in the 3D setting differed from that in the 2D standard assays (*SI Appendix*, Fig. S1 *D* and *E*). Dimethyldoxorubicin proved slightly less cytotoxic compared to doxorubicin, while azidodoxorubicin was most cytotoxic in 3D cultures (SI Appendix, Fig. S1D). Doxorubicinone was not cytotoxic in either system. The distribution of the different doxorubicin variants across the different spheroids was independent of the cell type tested (Fig. 2 and SI Appendix, Figs. S1 and S2).

Anthracycline Variants and Their Penetration in Spheroids. There are various conditions that may affect tissue or spheroid penetration of anthracyclines. First, we assessed the effect of time of exposure on anthracycline penetration of spheroids. We performed

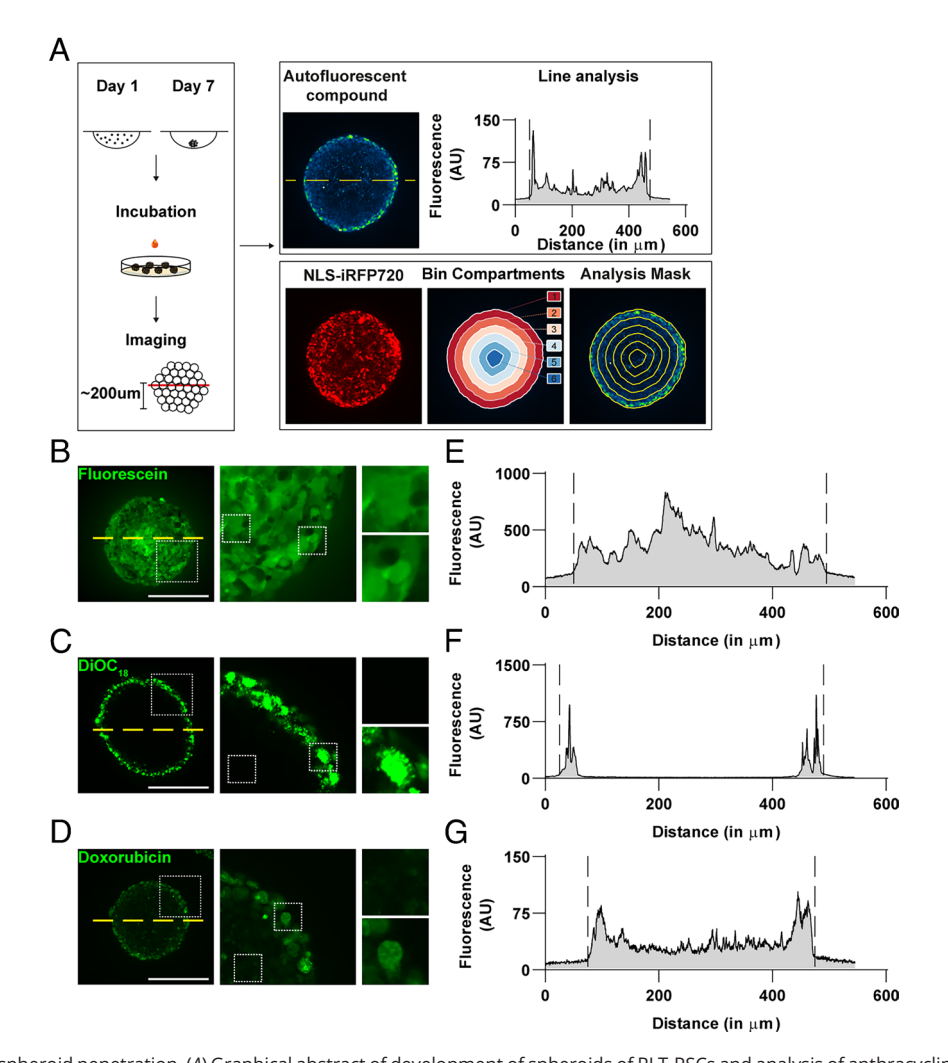


Fig. 1. Lipophilicity and spheroid penetration. (A) Graphical abstract of development of spheroids of RLT-PSCs and analysis of anthracycline uptake. RLT-PSCs were seeded in ultralow adherence plates to form spheroids. Day 7 cocultures were treated with anthracyclines and imaged using live cell spinning disc microscopy. (B) Representative images of penetration of free dye (Fluorescein) in spheroids exposed for 2 h. Fluorescence is shown in green false colors. Boxes indicate the zoom-in region shown on the Right of the figure. (Scale bar, 200 µm.) (C) Representative images of penetration lipophilic dye DiOC₁₈ in spheroids exposed for 2 h. Fluorescence is shown in green false colors. Boxes indicate the zoom-in region shown on the right of the figure. (Scale bar, 200 µm.) (D) Representative images of penetration doxorubicin in spheroids exposed for 2 h. Fluorescence is shown in green false colors. Boxes indicate the zoom-in region shown on the Right of the figure. (Scale bar, 200 µm.) (E) Distribution of Fluorescein in spheroids. A corresponding line plot is shown, with dashed vertical lines indicating the corresponding positions of the spheroid. (F) Distribution of DiOC₁₈ in spheroids. A corresponding line plot is shown, with dashed vertical lines indicating the corresponding positions of the spheroid. (G) Distribution of doxorubicin in spheroids. A corresponding line plot is shown, with dashed vertical lines indicating the corresponding positions of the spheroid.

time-lapse experiments with doxorubicin, dimethyldoxorubicin, and azidodoxorubicin, three drugs with different distributions in organoid-spheroid cocultures (SI Appendix, Fig. S1 A-C). Spheroids were exposed to $2 \mu M$ of the indicated drug and imaged every 10 min focused on an equatorial plan in the spheroid (Movies S1–S3). Fluorescence intensity is presented in false colors using an intensity lookup table (LUT) shown at the right (Fig. 3A). Drug penetration in spheroids reaches a plateau after 60 min (Fig. 3B) and did not further increase over time. Only fluorescence intensity in the spheroid periphery increased at later time points (Fig. 3 A and B). This was further illustrated by bin-analyses (Fig. 3C). Both dimethyldoxorubicin and azidodoxorubicin show peripheral uptake in spheroids within 30 min of drug exposure and increased spheroid penetration over time. Penetration in the spheroid interior is faster for azidodoxorubicin. while doxorubicin enters spheroids relatively slowly and penetrates their interior poorly (Fig. 3 A-C).

We then determined the effect of increasing the dose of doxorubicin and dimethyldoxorubicin on spheroid penetration, as in Fig. 3A. Spheroids were exposed to 0.5, 2.5, 5, or 10 μ M of the indicated anthracycline, and images were taken 2 h later. Surprisingly, up to 5 µM, distribution of the drug did not change, but the local concentration did. Only at 10 µM, a small yet significant increase of fluorescence in the spheroid's interior was seen (Fig. 3 D and E). Anthracyclines act by manipulating chromatin and thus must enter the nucleus for them to act (5). Therefore, we zoomed in on cells located in the spheroid periphery or interior and determined the location of the nucleus (marked by NLS-iRFP720) and doxorubicin (Fig. 3D). Line plots illustrate the distribution of both signals across these areas (up to 70 µm from the outside of the spheroid). Nuclear localization (red line) of the drug (gray line) was detectable only in the outer cells. Nuclear entry at deeper cell layers was detectable only at high concentrations of doxorubicin (Fig. 3F).

Dimethyldoxorubicin behaved differently. We saw no relative increase in anthracycline fluorescence in the spheroid interior at the different concentrations tested (Fig. 3 G and H). Although total fluorescence increases with concentration, the overall distribution did not change. While high-dose anthracyclines penetrate more deeply, most drug fluorescence is still captured in the outer

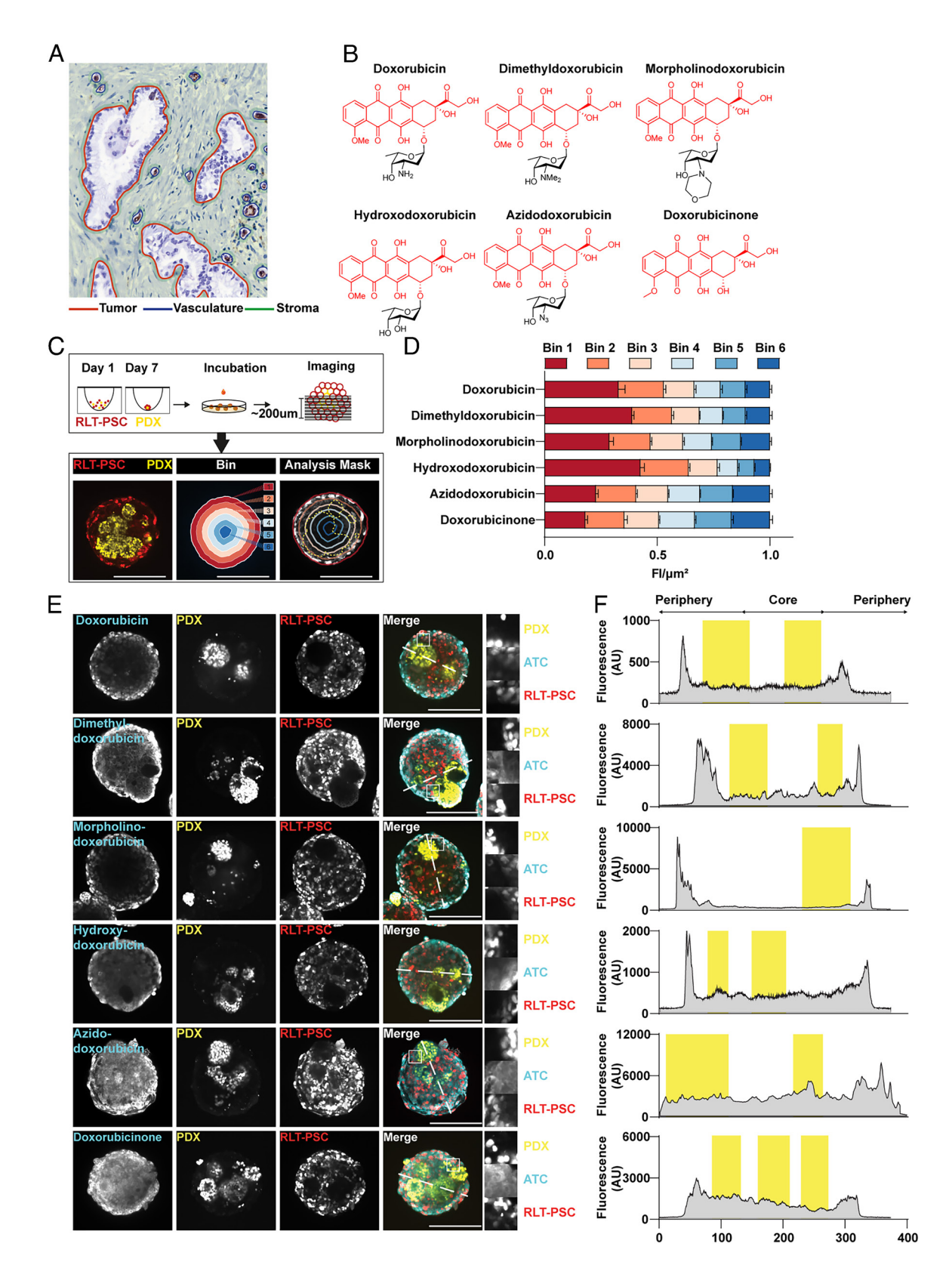


Fig. 2. Anthracycline penetration in pancreatic cancer organoid-fibroblast cocultures. (A) H&E staining with annotated area for tumor, stroma, and endothelium in pancreatic tumor. (B) Structures of anthracyclines used with the common aglycon (red) and the variable amino sugar group (black). (C) Graphical abstract of development of spheroids from RLT-PSCs and PDX cocultures and the microscopy analysis of anthracycline uptake. RLT-PSCs and PDX were mixed and seeded in ultralow adherence plates and incubated for coculture formation. Day 7 cocultures were treated with anthracyclines and imaged using live cell spinning disc microscopy. (D) Quantification of anthracycline penetration in the entire coculture calculated by relative fluorescence intensity normalized to bin area and shown as fraction of the total of all 6 bins. Cocultures were exposed to 10 μM of indicated anthracyclines in a medium at pH7.4 Fl/μm² (Fluorescence/micron²) (normalized to total fluorescence). Data represent three independent experiments and are presented as the mean with SEM (error bars). (E) Representative images of indicated anthracycline (cyan) penetration in RLT-PSCs (red) and PDX (yellow) cocultures. (Scale bar, 200 μm.) (F) Line plot analysis for the indicated anthracycline distribution (gray). The yellow box shows the location of PDX pancreatic tumor organoids within the cocultures. For all images, (Scale bar, 200 μm.)

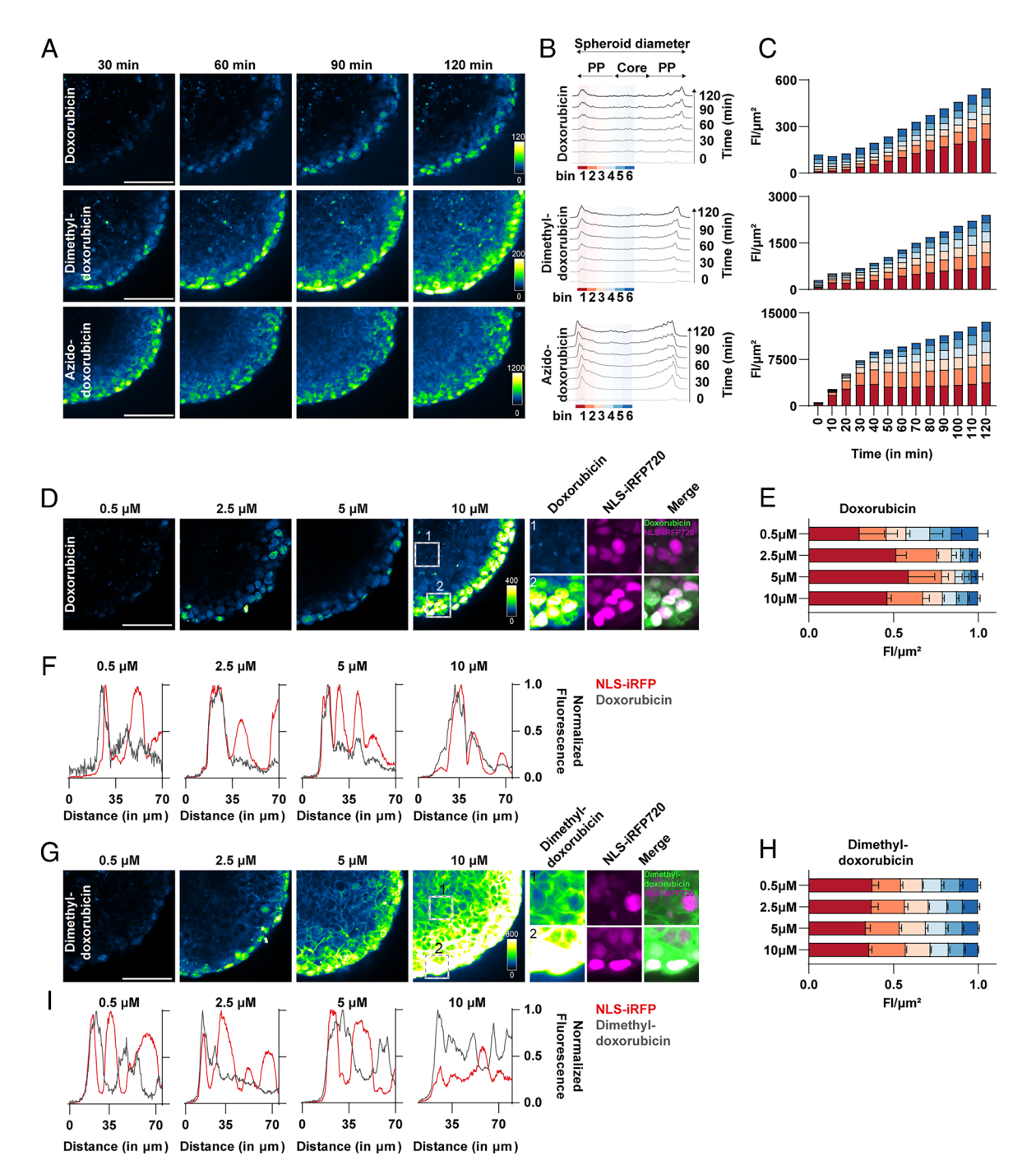
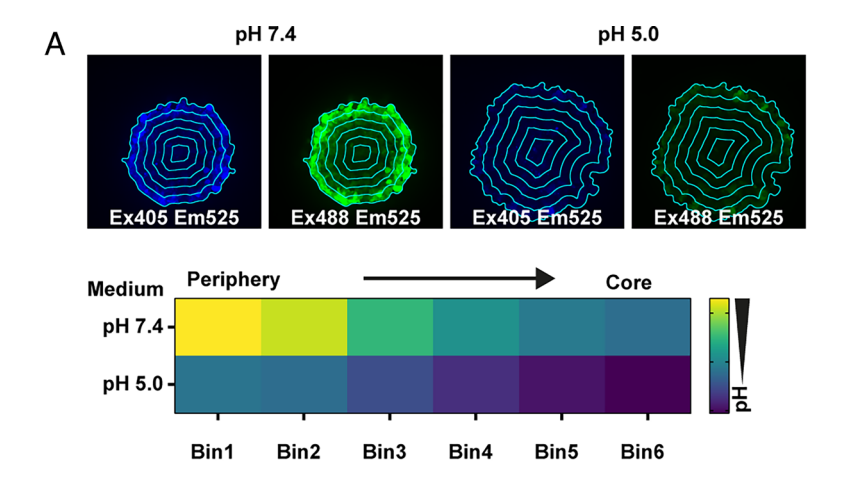


Fig. 3. Time and space differences of anthracycline exposure to spheroids. (A) Representative images (in false color LUTs) of anthracycline penetration with time. Spheroids were exposed to 2 µM of indicated anthracycline and imaged at 30-min intervals using live cell spinning disc microscopy. Time of imaging is indicated. (B) Individual line-plot analysis of fluorescent intensity spanning the whole spheroid diameter at 30-min intervals to visualize increase in peripheral and core fluorescence over time for the indicated anthracycline. Bins are indicated over distance for visual reference. (C) Fluorescence over time as determined using Bin analysis. (D) Representative images of dose escalation analysis showing penetration with increasing doses of doxorubicin. (Scale bar, 100 µm.) (E) Quantification of doxorubicin penetration calculated by relative fluorescence intensity normalized to bin area and shown as a fraction of the total 6 bins. Data represent three independent experiments and are presented as the mean with SEM (error bars). (F) Line plot analysis for the distribution of doxorubicin within the first 70 µm of spheroid and the iRFP720 nuclear signal at the indicated concentrations. (G) Representative images of dose escalation analysis showing penetration with increasing doses of dimethyldoxorubicin. (Scale bar, 100 µm.) (H) Quantification of dimethyldoxorubicin penetration calculated by relative fluorescence intensity normalized to bin area and shown as a fraction of the total 6 bins. Data represent three independent experiments and are presented as the mean with SEM (error bars). (I) Line plot analysis for the distribution of the dimethyldoxorubicin within the first 70 µm of spheroid and the iRFP720 nuclear signal at the indicated concentrations.

cell layers of the spheroid. Line plot analyses show NLS-iRFP720 (nucleus) and dimethyldoxorubicin normalized fluorescence at similar locations in the first outer cell layers. With exception of the first outer cell layers, dimethyldoxorubicin does not colocalize with the nucleus, but fluorescence is still detectable in the membrane or between the cells located deeper in the spheroid (Fig. 31).

Glycolytic Conditions Affect Cellular Uptake and Tissue Penetration of Weak Base Anthracyclines. Tissues are not homogeneous: tissue located at a distance from blood vessels will receive less oxygen. Consequently, cells at these locations increasingly rely on glycolysis to produce energy, exacerbated by the Warburg effect, prevalent in tumors. This produces lactate which acidifies the tissue microenvironment (27, 28). Spheroids may likewise reduce the pH in their interior (29). To test this, we expressed the ratiometric pH-sensitive probe SypHer3s on the cell surface of fibroblast cells to sense the pH in the microenvironment of the spheroids (30). The spheroids were cultured at physiological pH or pH 5.0 for 2 h, followed by ratiometric fluorescence measurements in the different bins (Fig. 4A). The ratio of fluorescence (indicating the pH across a spheroid cultured at pH7.4) for the different bins across the spheroid cultured at pH 7.4 showed that the pH in the spheroid interior is more acidic than in the periphery.

Anthracycline drugs are weak bases due to their single amine, which—when protonated—yields a positively charged molecule. Anthracyclines cross lipid bilayers that form the cell membranes by a flip-flop mechanism where a molecule moves from the outer lipid layer to the inner one while flipping the amino sugar through the hydrophobic lipid bilayer (31). If so, they are unlikely to traverse cell membranes when protonated, as the charge will be "excluded" from the hydrophobic inner core of the lipid bilayer. Lower pH increases the protonated state of the drug and will then limit cell entry. We first tested whether cellular uptake and cytotoxicity were affected when cells were exposed to different



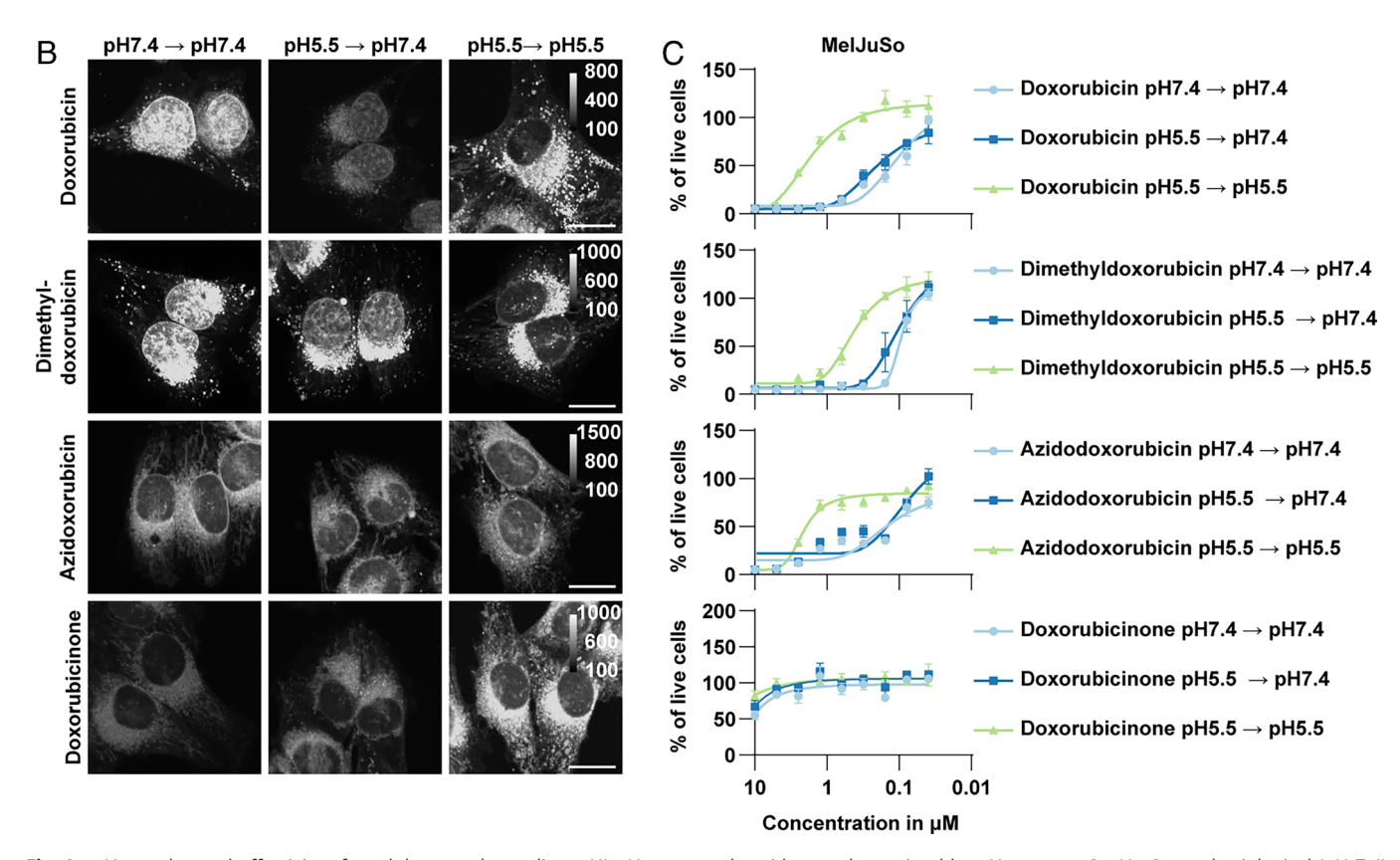


Fig. 4. pH, uptake, and effectivity of weak base anthracyclines. (*A*) pH across spheroids was determined by pH reporter SypHer3s at physiological (pH 7.4) medium conditions compared to acidic medium conditions of pH 5.0. Gradients in arbitrary units. (*B*) Uptake of anthracyclines indicated (in grey) in 2D cultured MelJuSo at pH 7.4 or pH 5.5 for 10 min at a concentration of 10 μ M analyzed following 40 min of incubation with indicated pH by live cell imaging. (Scale bar, 20 μ m.) (*C*) Dose–response experiments of the indicated compounds in MelJuSo cells. Cell death was read by a cell titer blue viability assay after cells had been exposed to the drugs at pH 7.4 or pH 5.5 for 2 h, followed by drug removal and further culture at pH 7.4 or pH 5.5 for 72 h. Data represent three independent experiments and are presented as the mean with SEM (error bars).

anthracyclines at different pH. While pancreatic cancer organoid cells dislike culture under acidic condition, we had to select cell lines able to grow under mildly acidic conditions. MelJuSo and HeLa cells tolerated 3 d of culture at pH 5.5 but not lower. We also verified that doxorubicin fluorescence was unaffected by pH (SI Appendix, Fig. S3 A and B). We exposed MelJuSo cells cultured in 2D for 10 min to 10 µM of the different anthracyclines at pH 5.5 or 7.4. We then removed the anthracyclines, followed by a 40 min culture at pH 7.4 or pH 5.5 and visualized anthracycline distribution by microscopy (Fig. 4B). Doxorubicin and dimethyldoxorubicin poorly entered the nucleus. Dimethyldoxorubicin accumulates in acidic endosomal/lysosomal compartments at pH 5.5, while doxorubicinone (which lacks the amino sugar moiety) poorly entered the nucleus independent of pH. Yet, doxorubicin, given to cells at pH 5.5, removed by washing and followed by transfer of the cells to pH7.4 for 40 min., did arrive in the nucleus. Cells exposed first to dimethyldoxorubicin at pH 5.5 before washing and shifting to pH 7.4 showed that the drug first entered lysosomal structures (which are acidic) before slowly entering the nucleus (Fig. 4B). Doxorubicin and dimethyldoxorubicin entered the nucleus of cells exposed to the drugs at pH 5.5 only when cultured subsequently at pH 7.4 but did so more slowly than in cells exposed and cultured at pH 7.4.

To test whether mildly acidic pH affects the cytotoxicity of anthracyclines, we performed a dose-response experiment under different pH conditions. MelJuSo or HeLa cells were exposed to different concentrations of the indicated anthracycline for 2 h at pH 5.5 or pH 7.4. Anthracyclines were then removed, and cells were further cultured for 3 d at either pH 7.4 or pH 5.5. The cytotoxicity of doxorubicin and dimethyldoxorubicin was strongly attenuated by exposure and culturing conditions at low pH when compared to cells maintained at pH 7.4 (Fig. 4C and SI Appendix, Fig. S3C). Drug exposure at pH 5.5 followed by washing and further culturing at pH 7.4 fully corrected the reduced drug activity seen at pH 5.5. The drugs are cell-associated at pH 5.5 but enter the cells more efficiently at pH 7.4. Mildly acidic conditions as in glycolytic tissues then function as a drug resistance mechanism.

The distribution of anthracyclines across a spheroid is nonlinear, with the majority of (nuclear) drug fluorescence in the outer few cell layers and an equal and lower intensity of drug fluorescence across the interior. To test whether this relates to cell entry and pH, we exposed spheroids to the different doxorubicin variants at pH 7.4 and pH 5.0 and monitored the fluorescence distribution in an equatorial plane by microscopy (Fig. 5). Acidification affected only the fluorescence distribution across spheroids for the protonated anthracyclines (doxorubicin and dimethyldoxorubicin), resulting in fairly equal distribution (Fig. 5 A and B). Zoom-in images of the spheroids' interior exposed to doxorubicin or dimethyldoxorubicin again showed a small fraction of the drugs entering the spheroids' interior, but not the nucleus (as marked by NLS-iRFP) (Fig. 5 A and B). We assessed spheroid penetration of other anthracyclines at different pH values. We included anthracyclines that cannot be protonated at the amino sugar. These included hydroxydoxorubicin, where the amine is replaced by an alcohol group, morpholinodoxorubicin and azidodoxorubicin where the amine will be more poorly protonated, and doxorubicinone lacking an amine (Fig. 2A). The distribution of these anthracyclines was indistinguishable at pH 5.5 and pH 7.4 (Fig. 5 E–H). Note that azidodoxorubicin and the poorly cytotoxic anthracycline doxorubicinone are already distributed equally across the spheroid, unlike morpholino- or hydroxydoxorubicin, which were efficiently taken up by the first few cell layers at both pH 7.4 and pH 5.0 (Fig. 5 E-H) (9).

Chemical Features Involved in Tissue Penetration of Anthracyclines. These different anthracyclines differ in their ability to penetrate spheroids. Can we infer the molecular features that control the rate of drug penetration in tissues and spheroids? We collected a series of anthracycline variants (9, 32, 33) and added the 6 anthracyclines in clinical use (SI Appendix, Table S1 and Fig. S4). Spheroids were exposed to the 37 different anthracyclines at $2 \mu M$ for 2 h and the drug distribution was imaged and analyzed as in the SI Appendix, Fig. S1 (Fig. 6A). Structural variants of anthracyclines yielded marked differences in distribution across spheroids, with some compounds showing an equal distribution across the spheroid volume and others entering only the outer spheroid cell layers.

We then zoomed into different regions within the spheroids to determine the intra- or intercellular localization of the different anthracyclines. We determined their location in the nucleus (nuc, colocalizing with NLS-iRFP720), in the cytoplasm (cyt), between cells (int), or not detectable (nd) for the different bins (Fig. 6 B and C). Most anthracyclines accumulated in the outer bins and were then located in the nucleus (Fig. 6C; red) while intracellular drug fluorescence in the more internal regions of the spheroid was usually poor or absent (Fig. 6C; green).

If the different anthracyclines distribute differently with respect to spheroid penetration, this must be determined by their particular chemical features. As a measure for tissue penetration, we used the relative fluorescence intensity detected in Bin 1, as a higher percentage of anthracycline in the outer layer related to poor penetration. Indeed, anthracyclines penetrating deep into the spheroid (such as doxorubicinone) did not accumulate in Bin1. Poorly penetrating anthracyclines (such as morpholinodoxorubicin) showed high relative fluorescence in Bin1 (Fig. 6A). Dimethyl- or diethyl modifications of the free amine group (lowering pKa) increases spheroid penetration (SI Appendix, Fig. S5A). Replacing the amine group by an azido- or hydroxy group (preventing protonation) also increased relative spheroid penetration (SI Appendix, Fig. S5B). Increasing hydrophilicity by adding multiple sugar moieties reduced uptake and penetration (SI Appendix, Fig. S5C), as did substituting the amine with pyrolidine or piperidine groups (SI Appendix, Fig. S5D). Complete removal of the amine (for a hydrogen atom) increased spheroid penetration (SI Appendix, Fig. S5E).

The series includes different anthracyclines with no, primary, or tertiary amines. This could be a determining feature for drug penetration. We grouped the drugs according to this difference (Fig. 6D). While a trend for relative fluorescence intensity detected in bin1 was observed, the correlation was only 0.41 and not statistically significant. Other features may be more important for tissue penetration. We calculated different features within the 37 anthracyclines tested by SwissADME (http://www.swissadme.ch/ index.php) (SI Appendix, Table S1) (34). In addition, we added features as determined by Chemaxon (https://chemaxon.com/) and the amine status. In total, we calculated 30 features for the different anthracycline variants with corresponding information as to the penetration in spheroids.

To determine the minimal number of features able to best describe the spheroid penetration, we used an "optimized" tree-model using the "fitrtree" MATLAB regression model (35, 36). This function calculates the minimal number of features that best describe the observed drug penetration and provides information on their relative contribution (Fig. 6E). Using all features in the prediction yielded a 14.37% error from the experimentally obtained values for spheroid penetration, which were mainly determined by three anthracyclines (DW906, MV181, and MV144) that showed a large prediction error (Fig. 6F). Three features within the anthracycline variants were calculated to best

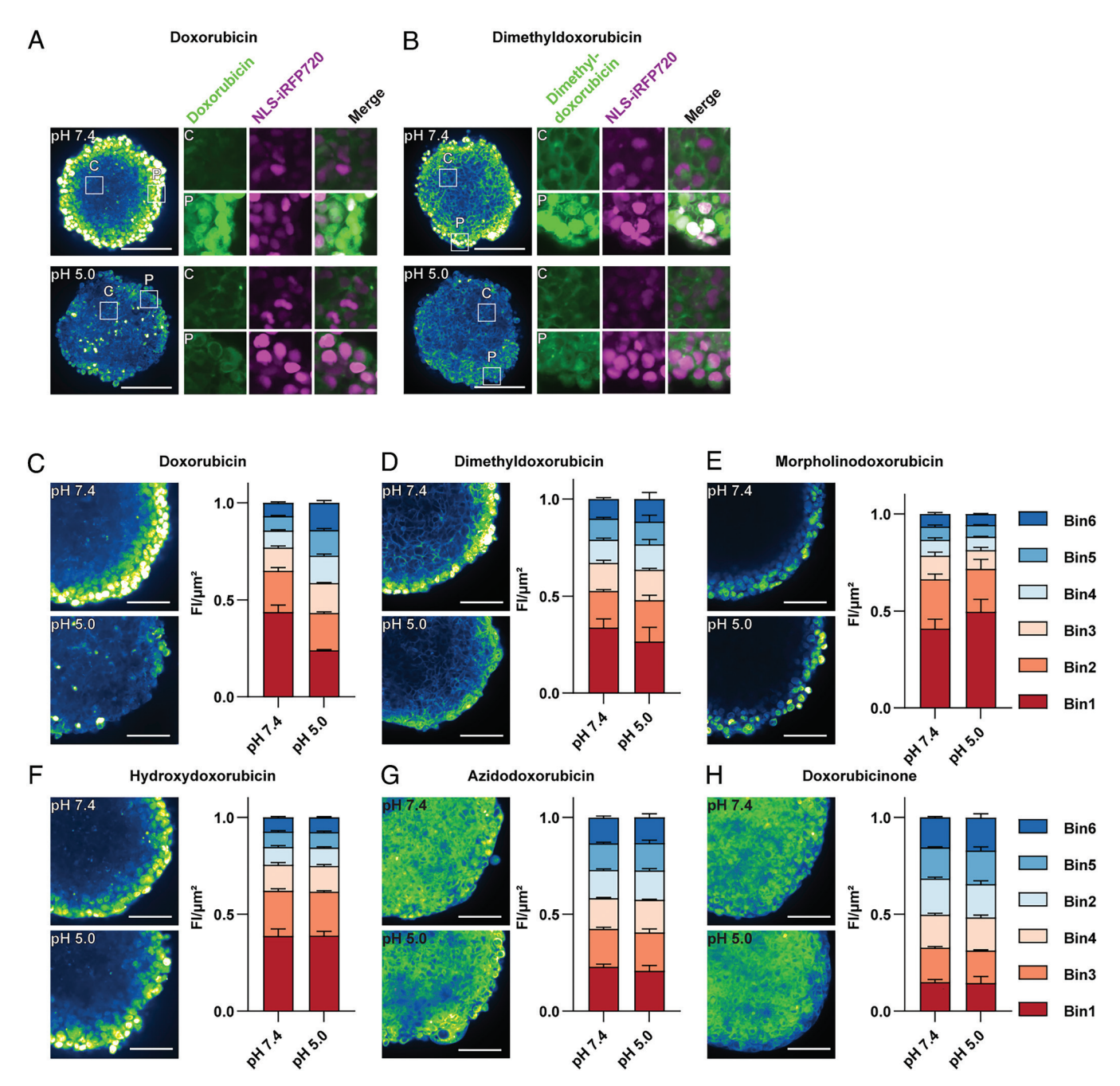


Fig. 5. pH and the distribution of weak base anthracyclines across spheroids. (A) Representative images including zoom-ins (as indicated) of spheroids exposed at 10 µM of doxorubicin in medium of pH 7.4 vs pH 5.0. An equatorial plane of spheroids was imaged after 2 h drug exposure by live cell imaging and analyzed. Fluorescence intensity shown in false colors as indicated by a color LUT. Insets show higher magnification of the localization of anthracyclines, P = peripheral and C =core. (Scale bar, 200 μm.) (B) Representative images including zoom-ins (as indicated) of spheroids exposed at 10 μM of dimethyldoxorubicin in medium of pH 7.4 vs pH 5.0. A middle plane of spheroids was imaged after 2 h drug exposure by live cell imaging and analyzed. Fluorescence intensity shown in false colors as indicated by a color LUT. Insets show higher magnification of the localization of anthracyclines, P = peripheral and C =core. (Scale bar, 200 µm.) (C) Representative image of 2 h spheroid penetration of 10 µM doxorubicin at different pH, as indicated. Relative fluorescence intensity normalized to bin area and shown as a fraction of the total 6 bins. (Scale bar, 100 µm.) Data represent three independent experiments and are presented as the mean with SEM (error bars). (D) Representative image of 2 h spheroid penetration of 10 µM dimethyldoxorubicin, at different pH, as indicated. Relative fluorescence intensity normalized to (*D*) Representative image of 2 h spheroid penetration of 10 µM dimethyldoxorubicin, at different pH, as indicated. Relative independent experiments and are presented as the mean with SEM (error bars). (*E*) Representative image of 2 h spheroid penetration of 10 µM azidodoxorubicin, at different pH, as indicated. Relative fluorescence intensity normalized to bin area and shown as a fraction of the total 6 bins. (Scale bar, 100 µm.) Data represent three independent experiments and are presented as the mean with SEM (error bars). (*F*) Representative image of 2 h spheroid penetration of 10 µM morpholinodoxorubicin, at different pH, as indicated. Relative fluorescence intensity normalized to bin area and shown as a fraction of the total 6 bins. (Scale bar, 100 µm.) Data represent three independent experiments and are presented as the mean with SEM (error bars). (*F*) Representative image of 2 h spheroid penetration of 10 µM doyorubicing at different pH, as indicated. are presented as the mean with SEM (error bars). (G) Representative image of 2 h spheroid penetration of 10 µM doxorubicinone, at different pH, as indicated. Relative fluorescence intensity normalized to bin area and shown as a fraction of the total 6 bins. (Scale bar, 100 µm.) Data represent three independent experiments and are presented as the mean with SEM (error bars). (H) Representative image of 2 hr spheroid penetration of doxorubicinone as in panels C-G. Quantification of three independent experiments is shown on the right and the different bins are shown as mean with SEM (error bars).

describe the spheroid penetration. These are the molar refractivity (MR), topological polar surface area (TPSA), and water solubility as calculated by Chemaxon (ChemaxonLogS) (Fig. 6E). When only the three dominant features were tested in combination, the

model had a 15.56% error related to the experimental data (Fig. 6G). This suggests that the addition of other features hardly improves the description of the anthracycline characteristics related to spheroid penetration.

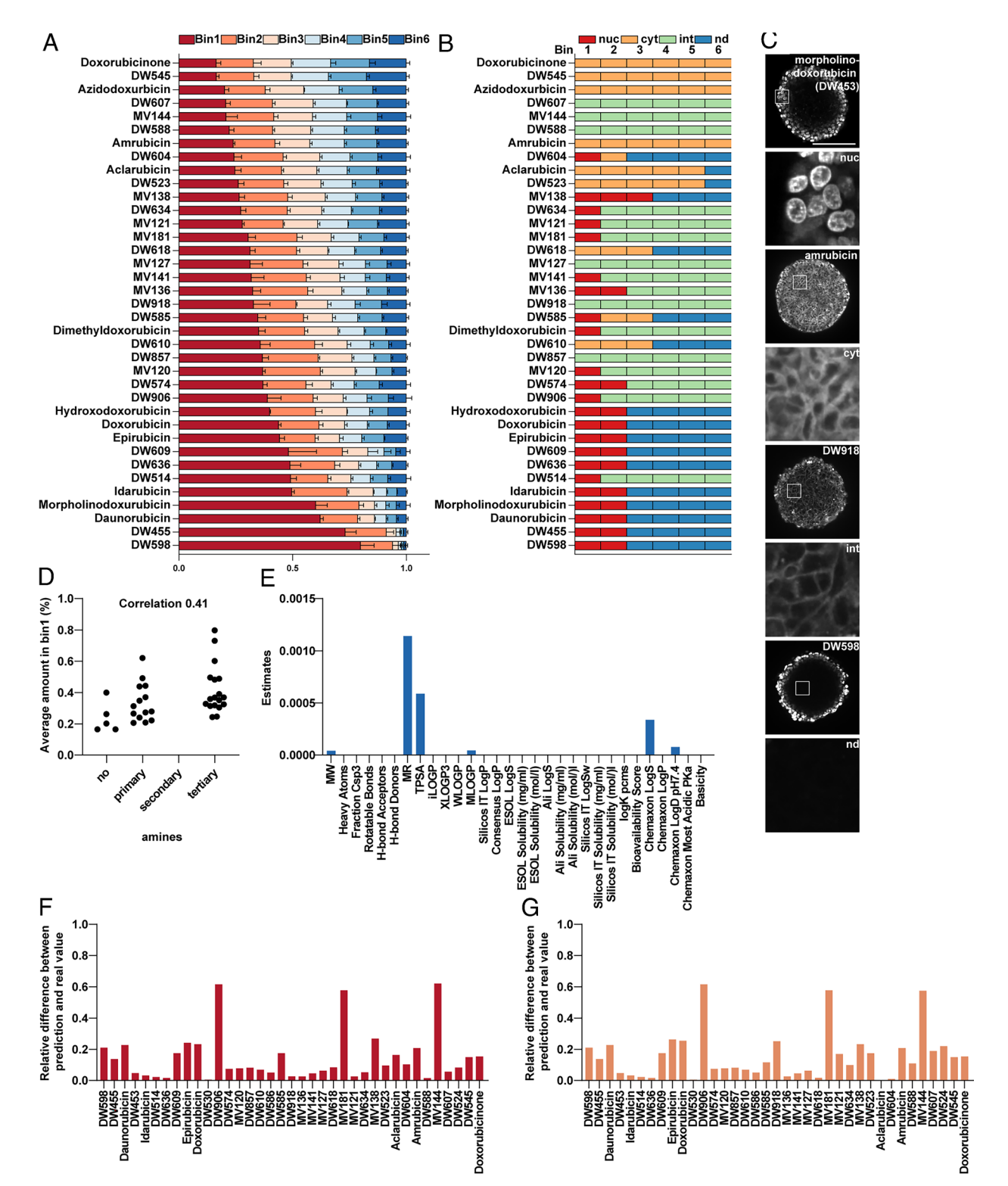


Fig. 6. Chemical variation of anthracyclines and penetration in a 3D spheroid penetration model to train predict molecules features and their performance for drug penetration. (A) Penetration in bins representing the different areas in the spheroid of the 37 anthracyclines after 2 h incubation (for structures SI Appendix, Fig. S4). Quantification of anthracycline penetration was calculated by relative fluorescence intensity normalized to bin area and shown as a fraction of the total of the 6 bins. Shown are mean with SEM of 4 to 7 independent spheroids. (B) Graphical summary of the four penetration patterns observed within our bin for 37 anthracyclines. (C) Representative images of cellular localization of anthracyclines. Nuc = nucleus, cyt = cytoplasm, int = intercellular/plasma membrane, nd = not determined. (Scale bar, 200 µm.) (D) Spheroid penetration as read by fluorescence in bin1 focused on the single amine within anthracyclines. The anthracycline variants were grouped according to the modification of the amine in the molecules. The normalized fluorescence in bin1 is depicted for the anthracycline variants lacking an amine (no), with a primary amine or with a tertiary amine. (E) 30 features for the anthracycline variants were tested for the best prediction of spheroid penetration (based on fluorescence in bin 1). In an iterative process, three key features and three minor features were calculated as optimal for predicting spheroid penetration. The features are indicated, and the y-axis depicts the predictor importance. (F) The deviation of the calculated penetration value (as fluorescence in bin1) compared to the experimental value. The code for the different compounds is shown on the x-axis and the relative difference between predicted and measured value (x100%) is shown on the y-axis. (G) The deviation between predicted and experimental value (based on fluorescence in bin1) now based on only the three major features as determined in Fig. 6F (MR, TPSA, and ChemaxonLogS). The different compounds are shown on the x-axis, and the relative difference between predicted and measured value (x100%) is shown on the y-axis.

Discussion

Drugs that fail to reach their target are ineffective. It is unclear how many potentially effective drugs may have failed due to poor tissue targeting. Understanding the mechanisms and rules of drug penetration in tissue would be highly beneficial for more effective drug development. Most drugs are not fluorescent and drug behavior at high resolution is then difficult to assess. Their tissue penetration may be followed by using chemically modified forms to selectively attach a detectable group by for example click chemistry. However, this may alter the behavior of the drug, as we show here for azidodoxorubicin. The best alternative to a fluorescence-based approach is to follow radioactive compounds (37) by micro-autoradiography of tissues, which provides accurate spatial information. Construction of a time series by autoradiography is cumbersome. For most drugs, the details of tissue penetrance are unclear. How distinctive features contribute to tissue penetration cannot be determined without systematic chemical modifications of the drug. Drug penetration must then be followed in high-throughput-high-resolution systems. We used a series of the fluorescent anthracyclines to study molecular features that drive tissue penetration (9, 32, 33). We used a spheroid model for high-resolution detection of drugs by time-lapse fluorescence microscopy. Spheroids mimic many aspects of tissue and comprise poorly oxygenated (glycolytic) acidified areas (38). Many drugs, including the anthracyclines, are weak bases. Their charge properties will be affected due to protonation under mildly acidic conditions. We show this for doxorubicin, a widely used cancer drug that fails to efficiently enter cells under acidic (glycolytic) conditions. Protonation of the single amine in doxorubicin likely limits membrane lipid bilayer flip-flop and cell entry, since variants lacking this single amine are not affected by mildly acidic pH. Lysosomes are also acidic and may function as a sink from which anthracyclines are slowly released for entry into the nucleus. In dose-response experiments, doxo- or dimethyldoxorubicin are considerably less efficient in eliminating cells when cultured at pH 5.5. However, they are equally effective after drug exposure at pH 5.5, followed by further drug-free culturing at pH 7.4, compared to cells that were exposed to drugs followed by drug-free culturing at pH 7.4. This suggests that the anthracyclines can associate with the cell membrane and resist removal at pH 5.5 but then enter and kill cells following neutralization. This identifies acidic (glycolytic) conditions as a physiological mechanism for resistance to anthracyclines and may help explain why pancreatic cancer is unresponsive to these drugs. Glycolysis may also upregulate the MDR1 drug exporter some two-fold to cause chemoresistance (39), but more efficient protonation of the single amine under acidic conditions to limit cellular uptake was not considered in this study. As indicated in our dose-response experiments at different pH, this will yield higher drug resistance. It was found that the extracellular pH is driving the increased doxorubicin accumulation and toxicity (40). Pancreatic cancer tissues are encapsulated by a fibroblast layer that separates blood vessels from the tumor. As a result, oxygenation of the tumor and its environment is poor and will result in a more glycolytic state. The acidified tumor microenvironment then prevents efficient entry of anthracyclines and contributes to drug resistance. This is also seen in the interior of pancreatic cancer organoids (41). Better treatment outcomes with these drugs may therefore be achieved by improving their tissue penetration and by addressing the glycolytic environment. Intracellular factors can further limit the distribution of doxorubicin. The low lysosomal pH will trap doxorubicin at that location and is reversible by an increase in lysosomal pH, for example, by using chloroquine and omeprazole or bicarbonate-based alkalinization (42). Neutralization of the intratumoral environment

in combination with doxorubicin to target pancreatic tumors is currently studied in Phase Ib/II clinical trials (NCT04203641), where L-DOS47, a urease conjugated to an anti-CEACAM6 antibody is used to increase pH by enzymatic conversion of urea to NH₃ and CO₂ (43). A retrospective study showed that neutralizing the pancreatic tumor microenvironment in combination with chemotherapy indeed improved overall survival (44). These different pathological features of cancer tissue should be considered for treatment decisions that involve anthracyclines and other weak base drugs. But it is important to note that the drugs still must penetrate various cell layers before getting to the pancreatic tumor. This will not be altered by neutralizing the glycolytic tumor microenvironment as the tumor is many cell layers away from the blood vessels that distribute the drugs across the body.

Various models have been developed to predict drug transport in silico in combination with in vitro testing (45-47). Hydrophilic molecules are readily distributed via the circulation and taken up by tissues or they diffuse simply between cells deeper into tissue, as we show for the distribution of fluorescein in spheroids. Lipophilic molecules tend to insert into the first membranes they encounter and usually do not diffuse beyond the first cell layer, at least in model systems (48). They can also bind to carriers such as albumin and be released to enter cells. However, many drugs have a relatively hydrophobic nature with some protonatable atoms (49). Anthracyclines must be in a membrane-solute equilibrium to allow acquisition by the next cell layer. Since these drugs are efficiently taken up by the cells, most drug will not be available beyond the first few cell layers, which explains the observed distribution of doxorubicin in spheroids. The drug exporter MDR1 prevents efficient cellular uptake. As a result, more drugs may be available for entering deeper into tissue, potentially at the cost of cytotoxicity at the outer cell layers. In the more internal glycolytic regions, the anthracyclines may then encounter an acidic environment where they will be more protonated at the cost of uptake by cells. If drugs then fail to enter cells, they can freely diffuse deeper in tissue, as we observed. Yet, the drugs are then also inactive as they fail to penetrate the cells' nuclei to initiate cell death programs. High doses of doxorubicin or dimethyldoxorubicin will allow somewhat deeper penetration, which may be a rationale for high-dose chemotherapy (50). High-dose chemotherapy with doxorubicin is usually performed at 2 to 3-fold higher than standard doses while mild acidification conditions (pH5.5) require a 20-fold increased concentration for optimal cytotoxicity. Consequently, high-dose chemotherapy for glycolytic tumor tissues does not result in improved tumor cytotoxicity but only produces more side effects, including cardiotoxicity (5, 51).

Can we predict and manipulate the rate of tissue penetration based on the molecular features of the drugs in question? There are three major features important for the penetration of anthracyclines. These include MR, which indirectly describes the electron distribution across a molecule. It includes the size and polarity of a molecule. Second, the TPSA reflects the combined polarity of a molecule and relates to their ability to permeate cells. Third, LogS is a measure for solubility of a molecule. Solubility indeed improves penetration (at the cost of cellular uptake) as does the polarity, as reflected by the penetration of fluorescein. Whether these features uniquely apply to tissue penetration of the anthracycline class of cancer drugs or are also applicable to other classes of small-molecule drugs is unclear. Still, consideration of these features may support the design of improved anthracyclines that penetrate more deeply into tissues and are active under glycolytic conditions for better treatment of pancreatic and other tumors.

The glycolytic pH in the tumor microenvironment can be a key factor that contributes to drug resistance. This observation can be used to improve the performance of anthracyclines. The amine of doxorubicin can be modified into a more acidic form, which will then less efficiently be protonated under glycolytic conditions, allowing efficient cell entry, as we show for morpholinodoxorubicin. Still, morpholinodoxorubicin is also absorbed at neutral pH by the outer cell layers of spheroids. Drugs then must be prevented from entering cells at neutral pH to be available to deeper tissues. pH-sensitive prodrugs may prevent cellular uptake at neutral pH and then deliver these drugs more deeply into tissues, in regions acidified by glycolysis where the prodrug is converted into an active drug for more selective elimination of tumor cells (52–54). Also packaging morpholinodoxorubicin in liposomes or other nanoparticles for tissue targeting may be a solution as morpholinodoxorubicin will enter and then eliminate (pancreatic cancer) cells growing under glycolytic conditions unlike doxorubicin. In vivo studies to further elucidate the penetration capacity of the different anthracyclines and rational modification of anthracycline cancer drugs based on our observations may yield different variants to control tumors that are unresponsive to conventional anthracyclines.

Materials and Methods

Anthracyclines and Other Chemicals. The anthracycline variants were synthesized, characterized, and described in detail before (9, 32). Doxorubicin was obtained from Accord Healthcare Limited, U.K., aclarubicin (sc-200160) was purchased from Santa Cruz Biotechnology, daunorubicin was obtained from Sanofi, idarubicin was obtained from Pfizer, and doxorubicinone was obtained from Santa Cruz Biotechnology. Fluorescein (L13251.36) and DiOC₁₈ (D275) were obtained from ThermoFisher. Fluorescein was dissolved in PBS at a stock solution of 10 mg/mL. $DiOC_{18}$ was dissolved at a stock solution of 1 mg/mL in DMSO. Both were stored at -70 °C until use.

Cell Culture, Spheroid Cultures, and Pancreatic Cancer Organoid-Spheroid Cocultures. MelJuSo cells were maintained in IMDM (Gibco) supplemented with 8% fetal bovine serum (FBS). HeLa cells and HEK293T cells were maintained using DMEM (Gibco) supplemented with 8% FBS. All cells were cultured at 37 °C and 5% CO₂. MelJuSo and HeLa cells were used for their ability to grow at a pH of 5.5.

RLT-PSC (24) were cultured at 37 °C and 5% CO₂ using DMEM (Gibco) supplemented with 8% FBS. Cells were stably transduced with a lentiviral plasmid expressing NLS-iRFP720 and hygromycin. Transduced cells were selected with 2 μg/mg hygromycin for 1 wk. The spheroid culture was generated using the hanging droplet method (55) on ultralow adherent plates. Spheroids were grown by plating 1,000 cells followed by a 7-d culture.

Collection and maintaining pancreatic tumor cells (PDX) were described by Harryvan et al. (56). In detail, this study used the PDO1 (Resection derived organoids PDO1 (HUB-08-B2-029B, PDAC) which were obtained from the Hubrecht Organoid Technology Biobank (HUB, Utrecht, The Netherlands) and subsequently transduced to stably express H2B-Cerulean3 as described (56). The PDX cells were maintained as spheroids in Matrigel in Advanced DMEM containing B27, Noggin, n-acetyl cysteine, Nicotinamide, Primocin, Gastrin, R-spo3, FGF10, A83-01, and WNT surrogate-Fc fusion protein, as described (26). Cocultures of RLT-PSC and PDX were made by combining 950 RLT-PSC with 50 PDX cells in a low-adherent plate in PDX media for 7 d with 1% Matrigel. Cells were regularly tested for Mycoplasma contamination and found negative.

For live experiments with acidified cultures, the pH of the DMEM containing FBS was adjusted by HCl and confirmed by measurements with a pH meter (Mettler Toledo SevenCompact).

Lentiviral Constructs and Transduction. The lentiviral plasmid was generated using restriction-based cloning. pLentiPGK Hygro DEST H2B-mCerulean3 (Addgene # 90234) served as backbone whereby the H2B-mCerulean was replaced by pNLS-iRFP720 (Addgene #45467) by subcloning using PCR methods. Lentivirus production was done using HEK293T cells. Similar amounts of

packaging plasmids expressing RRE, VSV-G, and REV were cotransfected with pLenti constructs. The virus was collected 5 d post-transfection and freshly used to stably transduce cells.

pH of spheroids was determined using the SypHer3s fluorescent ratiometric probe. The SypHer3s were subcloned into pLentiPGK Hygro as described above, following stable transduction into RLT-PSCs. The pH of the spheroids was determined using live cell microscopy following a previously described protocol (30).

Microscopy. For time-lapse live cell fluorescent microscopy, spheroids were grown over 7 d, placed in live cell dishes (Greiner) and imaged under conditions of 37 °C and 5% CO₂ by an Andor Dragonfly 500 spinning disk microscope. Data were collected using a $20 \times$ water immersion objective in a $2,048 \times 2,048$ format. Images were processed using Fiji. Detection of fluorescence is set such that saturation of the camera is prevented. The absence of detectable fluorescence does not imply the absence of anthracyclines as they may be there at low concentrations.

Viability Assays. The viability of 10 spheroids per experiment (performed in triplicate) was analyzed using Cell Titer Glo 3D following the manufacturer protocol (Promega). Spheroids were exposed to 10 μ M of defined anthracyclines for 2 h. Then, the medium was refreshed, and viability was assayed after 4 d. The viability of cells grown as monolayer was assessed using CellTiter-Blue (CTB assay) (Promega). Here, 2000 cells were treated for 2 h with drugs after which the drugs were removed and the cells were grown with refreshed media for 3 d. We used CellTiter Glo 3D for measuring the viability of cells in the 3D cultures because this method is more sensitive than the Cell Titer-Blue assay. For 2D cultures, the CellTiter-Blue assay was sufficiently effective, as the reagents could more easily penetrate the cells in 2D.

Data Processing and Analysis. A macro was written in Fiji to perform fluorescence quantification across different bins in the spheroids. Mask of outline of spheroid of single z-stack was determined. Spheroid was divided in 6 bins. Total fluorescence was determined and normalized to fluorescence per μ m². To normalize between different anthracyclines with different fluorescent intensities, fluorescence was normalized to total drug fluorescence as detected in a single spheroid z-stack.

Determining Drug Penetration Features. To be able to predict the behavior of new compounds, characteristic traits of compounds were assessed using MATLAB. A sequential feature selection mechanism ("sequentialfs" function of MATLAB) was used. This analysis shows which (combination of) characteristic traits (SI Appendix, Table S1) best predict the percentage of compound left in layer 1 for the different compounds (*SI Appendix*, Table S1). The sequential feature selection analysis was used on the features of the 37 different anthracycline analogs (http:// www.swissadme.ch/index.php and https://chemaxon.com/) (34). The sequentialfs function selects a subset of the 25 features by sequentially selecting features until the prediction does not improve further. In each iteration, a regression binary decision tree is fit (using "fitrtree" function in MATLAB) to predict the percentage of the compound in layer 1, using the features selected by the sequentialfs function (36). With use of the "loss" function in MATLAB, the quality of the binary decision tree model is calculated. The lower the loss value, the better the prediction.

Data, Materials, and Software Availability. All study data are included in the article and/or supporting information.

ACKNOWLEDGMENTS. We thank the Neefjes lab members for their comments and suggestions. This work was supported by grants from the Oncode Institute and the Institute of Chemical Immunology to Jacques Neefjes and Herman Overkleeft and Hersenstichting to Erik Abels and Marike Broekman.

Author affiliations: ^aDepartment of Cell and Chemical Biology and Oncode Institute, Leiden University Medical Center, Leiden 2300 RC, The Netherlands; ^bLeiden Institute of Chemistry, Faculty of Science, Leiden University, Leiden 2333 RC, The Netherlands; ^cDepartment of Neurosurgery, Leiden University Medical Center, Leiden 2300 RC, The Netherlands; and ^dDepartment of Neurosurgery, Haaglanden Medical Center, The Hague 2512 VA, The Netherlands

Author contributions: E.R.A., H.S.O., M.L.D.B., and J.N. designed research; E.R.A., E.t.L., and S.Y.v.d.Z. performed research; L.J., M.H., H.S.O., and S.Y.v.d.Z. contributed new reagents/ analytic tools; E.R.A., E.t.L., J.H.T.R., L.M.V., and J.N. analyzed data; and E.R.A. and J.N. wrote

- A. I. Minchinton, I. F. Tannock, Drug penetration in solid tumours. Nat. Rev. Cancer 6, 583-592 (2006).
- M. W. Dewhirst, T. W. Secomb, Transport of drugs from blood vessels to tumour tissue. Nat. Rev. Cancer
- R. H. Grantab, I. F. Tannock, Penetration of anticancer drugs through tumour tissue as a function of cellular packing density and interstitial fluid pressure and its modification by bortezomib. BMC Cancer 12, 214 (2012).
- G. Minotti, P. Menna, E. Salvatorelli, G. Cairo, L. Gianni, Anthracyclines: Molecular advances and pharmacologic developments in antitumor activity and cardiotoxicity. Pharmacol. Rev. 56, 185-229
- S.Y. van der Zanden, X. Qiao, J. Neefjes, New insights into the activities and toxicities of the old anticancer drug doxorubicin. FEBS J. 288, 6095–6111 (2021).
- X. Qiao et al., Diversifying the anthracycline class of anti-cancer drugs identifies aclarubicin for superior survival of acute myeloid leukemia patients. Mol. Cancer 23, 120 (2024).
- X. Qiao et al., Uncoupling DNA damage from chromatin damage to detoxify doxorubicin. Proc. Natl. Acad. Sci. U. S. A. 117, 15182–15192 (2020).
- J. Neefjes, K. Gurova, J. Sarthy, G. Szabó, S. Henikoff, Chromatin as an old and new anticancer target Trends Cancer 10, 696-707 (2024).
- M. A. van Gelder et al., Re-exploring the anthracycline chemical space for better anti-cancer compounds. J. Med. Chem. 66, 11390-11398 (2023).
- M. A. van Gelder et al., Novel N, N-dimethyl-idarubicin analogues are effective cytotoxic agents for ABCB1-overexpressing. Doxorubicin-resistant cells. J. Med. Chem. 67, 13802-13812 (2024).
- E. S. Nakasone et al., Imaging tumor-stroma interactions during chemotherapy reveals contributions of the microenvironment to resistance. Cancer Cell 21, 488-503 (2012).
- J. Lankelma et al., Doxorubicin gradients in human breast cancer. Clin. Cancer Res. 5, 1703-1707 (1999).
- J. L. Au et al., Determinants of drug delivery and transport to solid tumors. J. Control. Release. 74, 31-46 (2001).
- H. Maeda, J. Wu, T. Sawa, Y. Matsumura, K. Hori, Tumor vascular permeability and the EPR effect in macromolecular therapeutics: A review. *J. Control. Release.* **65**, 271–284 (2000).
- C. D. Arvanitis et al., Mechanisms of enhanced drug delivery in brain metastases with focused ultrasound-induced blood-tumor barrier disruption. Proc. Natl. Acad. Sci. U. S. A. 115, E8717-e8726
- V. Khosrawipour et al., Effect of irradiation on tissue penetration depth of doxorubicin after pressurized intra-peritoneal aerosol chemotherapy (PIPAC) in a novel ex-vivo model. J. Cancer. 7,
- 17. J. H. Zheng, C.-T. Chen, J. L. S. Au, M. G. Wientjes, Time-and concentration-dependent penetration of doxorubicin in prostate tumors. AAPS PharmSci. 3, 15 (2001).
- A. Sajid et al., Synthesis and characterization of Bodipy-FL-cyclosporine A as a substrate for multidrug resistance-linked P-glycoprotein (ABCB1). Drug Metab. Dispos. 47, 1013–1023 (2019).
- N. el Tayar et al., Solvent-dependent conformation and hydrogen-bonding capacity of cyclosporin A: Evidence from partition coefficients and molecular dynamics simulations. J. Med. Chem. 36, 3757-3764 (1993).
- C. K. Hirt, et al., Drug screening and genome editing in human pancreatic cancer organoids identifies drug-gene interactions and candidates for off-label treatment. Cell Genom. 2, 100095
- K. Schlick et al., Non-pegylated liposomal doxorubicin as palliative chemotherapy in pre-treated advanced pancreatic cancer: A retrospective analysis of twenty-eight patients. Technol. Cancer Res Treat. 20, 15330338211042139 (2021).
- D. Murthy et al., Cancer-associated fibroblast-derived acetate promotes pancreatic cancer development by altering polyamine metabolism via the ACSS2-SP1-SAT1 axis. Nat. Cell Biol. 26, 613-627 (2024).
- 23. M. H. Sherman, M. P. di Magliano, Cancer-associated fibroblasts: Lessons from pancreatic cancer. Annu. Rev. Cancer Biol. 7, 43-55 (2023).
- R. Jesnowski et al., Immortalization of pancreatic stellate cells as an in vitro model of pancreatic fibrosis: Deactivation is induced by matrigel and N-acetylcysteine. Lab. Invest. 85, 1276-1291 (2005).
- S. Eksborg, Pharmacokinetics of anthracyclines. *Acta Oncol.* **28**, 873–876 (1989). E. Driehuis, A. Gracanin, R. G. J. Vries, H. Clevers, S. F. Boj, Establishment of pancreatic organoids from normal tissue and tumors. *STAR Protoc.* **1**, 100192 (2020), 10.1016/j.xpro.2020.100192.
- C. J. Halbrook, C. A. Lyssiotis, M. Pasca di Magliano, A. Maitra, Pancreatic cancer: Advances and challenges. Cell 186, 1729-1754 (2023).
- M. C. De Santis, B. Bockorny, E. Hirsch, P. Cappello, M. Martini, Exploiting pancreatic cancer metabolism: Challenges and opportunities. Trends Mol. Med. 30, 592-604 (2024).

- 29. E. V. Zagaynova et al., "Imaging of Intracellular pH in tumor spheroids using genetically encoded sensor SypHer2" in Multi-Parametric Live Cell Microscopy of 3D Tissue Models, R. I. Dmitriev, Ed. (Springer International Publishing, Cham, 2017), pp. 105-119. 10.1007/978-3-319-67358-5_7.
- Y. G. Ermakova et al., SypHer3s: A genetically encoded fluorescent ratiometric probe with enhanced brightness and an improved dynamic range. Chem. Commun. 54, 2898-2901 (2018).
- T. J. Yacoub, A. S. Reddy, I. Szleifer, Structural effects and translocation of doxorubicin in a DPPC/Chol bilayer: The role of cholesterol. Biophys. J. 101, 378-385 (2011).
- D. P. A. Wander *et al.*, Synthetic (N, N-dimethyl)doxorubicin glycosyl diastereomers to dissect modes of action of anthracycline anticancer drugs. *J. Org. Chem.* **86**, 5757–5770 (2021).

 D. P. A. Wander *et al.*, Doxorubicin and aclarubicin: Shuffling anthracycline glycans for improved
- anticancer agents. J. Med. Chem. 63, 12814–12829 (2020).
- A. Daina, O. Michielin, V. Zoete, SwissADME: A free web tool to evaluate pharmacokinetics, drug-likeness and medicinal chemistry friendliness of small molecules. Sci. Rep. 7, 42717 (2017).
- L. Breiman, J. Friedman, C. J. Stone, R. A. Olshen, Classification and Regression Trees (Taylor & Francis, 1984).
- The MathWorks Inc., MATLAB version: 9.10.0 (R2021a) Update 8 (The MathWorks Inc., Natick, MA,
- E. G. Solon, Autoradiography techniques and quantification of drug distribution. Cell Tissue Res. 360, 87-107 (2015).
- Y. Kato et al., Acidic extracellular microenvironment and cancer. Cancer Cell Int. 13, 89 (2013).
- W. Wagner, K. D. Kania, A. Blauz, W. M. Ciszewski, The lactate receptor (HCAR1/GPR81) contributes to doxorubicin chemoresistance via ABCB1 transporter up-regulation in human cervical cancer HeLa cells. J. Physiol. Pharmacol. 68, 555-564 (2017).
- 40. L. E. Gerweck, S. V. Kozin, S. J. Stocks, The pH partition theory predicts the accumulation and toxicity of doxorubicin in normal and low-pH-adapted cells. Br. J. Cancer 79, 838-842 (1999).
- A. Stigliani et al., Adaptation to an acid microenvironment promotes pancreatic cancer organoid growth and drug resistance. *Cell Rep.* **43**, 114409 (2024).

 C. M. Lee, I. F. Tannock, Inhibition of endosomal sequestration of basic anticancer drugs: Influence
- on cytotoxicity and tissue penetration. *Br. J. Cancer* **94**, 863–869 (2006).

 B. V. Jardim-Perassi *et al.*, L-DOS47 elevates pancreatic cancer tumor pH and enhances response to
- immunotherapy. Biomedicines 12, 461 (2024).
- R. Hamaguchi, R. Narui, H. Wada, Effects of alkalization therapy on chemotherapy outcomes in metastatic or recurrent pancreatic cancer. Anticancer Res. 40, 873-880 (2020).
- C. J. Evans et al., A mathematical model of doxorubicin penetration through multicellular layers. J. Theor. Biol. 257, 598-608 (2009).
- C. M. Groh et al., Mathematical and computational models of drug transport in tumours. J. R. Soc. Interface 11, 20131173 (2014).
- J. Liu et al., A novel individual-cell-based mathematical model based on multicellular tumour spheroids for evaluating doxorubicin-related delivery in avascular regions. Br. J. Pharmacol. 174, 2862-2879 (2017).
- 48. A. H. Kyle, L. A. Huxham, A. S. Chiam, D. H. Sim, A. I. Minchinton, Direct assessment of drug penetration into tissue using a novel application of three-dimensional cell culture. Cancer Res. 64, 6304-6309 (2004).
- C. A. Lipinski, F. Lombardo, B. W. Dominy, P. J. Feeney, Experimental and computational approaches to estimate solubility and permeability in drug discovery and development settings. Adv. Drug Deliv. Rev. 46, 3-26 (2001).
- J. E. Ferguson, D. J. Dodwell, A. M. Seymour, M. A. Richards, A. Howell, High dose, dose-intensive chemotherapy with doxorubicin and cyclophosphamide for the treatment of advanced breast cancer. Br. J. Cancer 67, 825-829 (1993).
- A. H. Honkoop et al., Dose-intensive chemotherapy with doxorubicin, cyclophosphamide and GM-CSF fails to improve survival of metastatic breast cancer patients. Ann. Oncol. 7, 35-39 (1996).
- Z. Ahmed et al., Increasing chemotherapeutic efficacy using pH-modulating and doxorubicinreleasing injectable chitosan-poly(ethylene glycol) hydrogels. ACS Appl. Mater. Interfaces 15, 45626-45639 (2023).
- Z.-H. Jin *et al.*, Evaluation of doxorubicin-loaded pH-sensitive polymeric micelle release from tumor blood vessels and anticancer efficacy using a dorsal skin-fold window chamber model. *Acta* Pharmacol. Sin. 35, 839-845 (2014).
- J.-Z. Du, X.-J. Du, C.-Q. Mao, J. Wang, Tailor-made dual pH-sensitive polymer-doxorubicin nanoparticles for efficient anticancer drug delivery. J. Am. Chem. Soc. 133, 17560-17563 (2011).
- R. Foty, A simple hanging drop cell culture protocol for generation of 3D spheroids. J. Vis. Exp. 6, 2720 (2011). 10.3791/2720.
- T. J. Harryvan et al., A novel pancreatic cancer mini-tumor model to study desmoplasia and myofibroblastic cancer-associated fibroblast differentiation. Gastro. Hep. Adv. 1, 678-681 (2022).